The Astrophysical Journal, 708:913–919, 2010 January 10 doi:10.1088/0004-637X/708/2/913

LARGE-SCALE EXTREME-ULTRAVIOLET DISTURBANCES ASSOCIATED WITH A LIMB CORONAL MASS EJECTION

Y. Dai[1,2], F. Auchère[1], J.-C. Vial[1], Y. H. Tang[2], and W. G. Zong[3]
[1] Institut d'Astrophysique Spatiale, Bât. 121, Université Paris XI and CNRS, 91405 Orsay, France; yu.dai@ias.u-psud.fr
[2] Department of Astronomy, Nanjing University, Nanjing 210093, China
[3] National Center for Space Weather, China Meteorological Administration, Beijing 100081, China
Received 2009 July 30; accepted 2009 October 26; published 2009 December 16

ABSTRACT

We present composite observations of a coronal mass ejection (CME) and the associated large-scale extreme-ultraviolet (EUV) disturbances on 2007 December 31 by the Extreme-ultraviolet Imager (EUVI) and COR1 coronagraph on board the recent *Solar Terrestrial Relations Observatory* mission. For this limb event, the EUV disturbances exhibit some typical characteristics of EUV Imaging Telescope waves: (1) in the 195 Å bandpass, diffuse brightenings are observed propagating oppositely away from the flare site with a velocity of ∼260 km s^{-1}, leaving dimmings behind; (2) when the brightenings encounter the boundary of a polar coronal hole, they stop there to form a stationary front. Multi-temperature analysis of the propagating EUV disturbances favors a heating process over a density enhancement in the disturbance region. Furthermore, the EUVI–COR1 composite display shows unambiguously that the propagation of the diffuse brightenings coincides with a large lateral expansion of the CME, which consequently results in a double-loop-structured CME leading edge. Based on these observational facts, we suggest that the wave-like EUV disturbances are a result of magnetic reconfiguration related to the CME liftoff rather than true waves in the corona. Reconnections between the expanding CME magnetic field lines and surrounding quiet-Sun magnetic loops account for the propagating diffuse brightenings; dimmings appear behind them as a consequence of volume expansion. X-ray and radio data provide us with complementary evidence.

Key words: Sun: corona – Sun: coronal mass ejections (CMEs) – Sun: magnetic fields – Sun: UV radiation

1. INTRODUCTION

The discovery of global coronal waves by the Extreme-ultraviolet Imaging Telescope (EIT; Delaboudinière et al. 1995) on board the *Solar and Heliospheric Observatory* (*SOHO*) satellite (hence named EIT or extreme-ultraviolet (EUV) wave) in the late 1990s re-sparked the interest in large-scale disturbances in the solar atmosphere. Disturbance evidence first came from flare-related Moreton waves (Moreton 1960; Moreton & Ramsey 1960) in chromospheric Hα filtergrams whose observation history can date back to half a century ago. Moreton waves appear as a semicircular front moving away from the flare site with velocities of 500–2000 km s^{-1}. Since in the dense chromosphere no wave mode can maintain such high velocities, Uchida (1968) modeled Moreton waves as the skirt of a coronal fast-mode magnetohydrodynamic (MHD) wave that sweeps the chromosphere. In a simple magnetic environment, EIT waves also have the appearance of an almost circular wave front followed by expanding dimming regions (Thompson et al. 1998, 1999). Although much more diffuse in morphology, in some cases the EIT wave fronts were observed cospatial with an Hα Moreton wave front (Thompson et al. 2000b; Khan & Aurass 2002). Therefore, the interpretation of EIT waves as a fast-mode wave which also acts as the coronal counterpart of a Moreton wave has been naturally proposed (Wang 2000; Ofman & Thompson 2002; Warmuth et al. 2004). In the wave model, some characteristics of EIT waves, including the slow expansion rates (Wang 2000), stopping near coronal holes (CHs; Thompson et al. 1999) and reflection/refraction by active regions (ARs; Ofman & Thompson 2002; Veronig et al. 2006), can be well explained.

However, the velocities of EIT waves, 170–350 km s^{-1} as reported by Klassen et al. (2000) in a statistical study, are only one-third of those of Moreton waves. In order to overcome the velocity discrepancy in the two EUV/Moreton wave events, Warmuth et al. (2001) proposed that a flare-powered coronal pulse, which is initially strong enough to perturb the chromosphere at its skirt, may decelerate into the observed velocity range of EIT waves as the wave strength dissipates progressively and then cannot produce significant chromospheric perturbations any more. But in another event Eto et al. (2002) found that the Moreton wave triggered oscillations of a remote filament earlier than the arrival of the corresponding EIT wave at the oscillation site, strongly against the common origin scenario. Recent statistical results have shown that EIT waves are more closely associated with coronal mass ejections (CMEs) than with flares (Biesecker et al. 2002; Cliver et al. 2005; Chen 2006). Although the possibility of EIT waves being freely propagating, large-amplitude MHD simple waves temporarily powered by the lateral expansion of a CME (Veronig et al. 2008) cannot be ruled out, some other authors have alternatively modeled them as a pseudo wave related to the CME liftoff, which is either due to Joule heating (Delannée 2000) or density enhancement (Chen et al. 2002, 2005) associated with successive opening of magnetic field lines overlying the CME flux rope, or caused by interaction of the CME field lines with surrounding magnetic loops (Attrill et al. 2007). Besides, Wills-Davey et al. (2007) claim EIT waves to be a type of coronal MHD soliton whose velocity is also dependent on the amplitude of the pulse in addition to properties of the transmission medium. Nevertheless, current observations are unable to distinguish between soliton and non-soliton waves yet.

The issue whether EIT waves are true waves or not remains open for debate, and thus it deserves further attention. EIT waves are best observed when initiated from an on-disk site. On the other hand, observations of EIT waves close to the limb permit us to link the low coronal disturbances to the magnetic configuration of the CME (Zhukov & Auchère 2004). Such an

unambiguous correlation relies on simultaneous observations which cover the whole corona without spatial gap. During the *SOHO* mission, some composite observations of the inner–outer corona have already been employed to study the early phase of CMEs (Aurass et al. 1999; Maia et al. 1999; Thompson et al. 2000a; Ko et al. 2003). Unfortunately, the temporal limitations of the previous observations make them unable to synchronously trace the evolution of a CME and the associated EUV wave for a necessarily long time. Thanks to their sufficiently high temporal resolutions and continuous spatial coverage, the EUV Imager (EUVI; Wuelser et al. 2004) and COR1 coronagraph (Thompson et al. 2003) on board the recent *Solar Terrestrial Relations Observatory* (*STEREO*; Kaiser et al. 2008) mission are suitable for such tasks. In this paper, we present EUVI–COR1 composite observations of a limb CME and the associated wave-like EUV disturbances on 2007 December 31. In Section 2, we analyze the *STEREO* observations and complementary X-ray and radio data. The results are discussed in Section 3 and conclusions are drawn in Section 4.

2. OBSERVATIONS AND DATA ANALYSIS

Starting from ∼00:35 UT on 2007 December 31, NOAA AR 10980 produced a CME/flare event when it was still limb-occulted at Earth viewpoint. Extrapolating the location of the AR from its appearance on the disk in the following days suggests that the flare site was at ∼10° behind the eastern limb at the time of the event.

EUVI and COR1 are part of the Sun–Earth Connection Coronal and Heliospheric Investigation (SECCHI; Howard et al. 2008) instrument suite on board *STEREO*. EUVI observes the chromosphere and low corona up to 1.7 $R_\odot$ in four EUV bandpasses (304, 171, 195, and 284 Å) with a spatial resolution of ∼1.″6 pixel^{-1}. As the inner one of two onboard Lyot coronagraphs, COR1 observes CMEs from 1.5 to 4 $R_\odot$ with a spatial resolution of ∼7.″5 pixel^{-1}. During the period of interest, the cadences of EUVI were 2.5, 10, and 20 minutes for the 171, 195–304, and 284 Å bandpass, respectively, while COR1 obtained one image every 5 minutes.

STEREO is composed of two identical spacecraft orbiting the Sun ahead (*S/C A*) and behind (*S/C B*) the Earth near the ecliptic plane. Since the end of 2007 January, the *STEREO* twin spacecraft have been continuously separating. Their coordinate information on the event date is listed in Table 1. By use of the coordinate parameters, a pre-event EUVI 195 Å image pair at 00:25:38 UT[4] was prepared with the Solar Software routine `scc_stereopair.pro` (Figure 1). The large enough separation of *S/C B* and the Earth, 22.°8, ensured that the limb-occulted source region as viewed from the Earth was seen in the field of view (FOV) of *S/C B*, while at *S/C A* viewpoint it was further occulted behind the limb. Hence, the following data description mainly relies on *S/C B* observations. As shown in Figure 1, the overall coronal environment before the event was rather simple under solar minimum conditions. The AR was located close to the eastern limb and slightly south of the equator; loops extending out from it were seen off-limb. Besides two polar CHs there was an equatorial CH west to the AR, with the rest of the disk dominated by quiet Sun (QS).

[4] Due to the difference in light-travel time from the Sun to each spacecraft, *STEREO* image pairs are taken at slightly different times to correspond to the same time on the Sun. In this paper, all *STEREO* observation times are corrected to Earth UT to enable direct comparison with near-Earth observations.

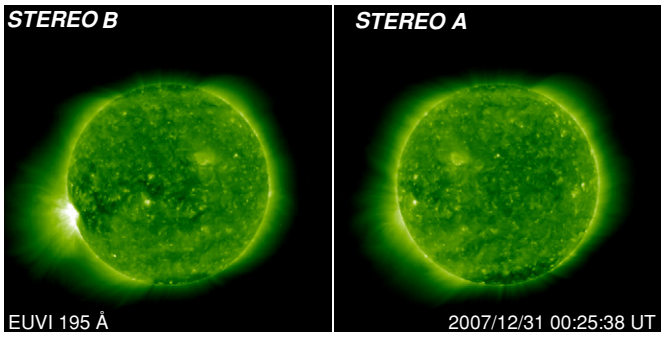

Figure 1. Simultaneous EUVI 195 Å images (the left panel for *S/C B* and the right panel for *S/C A*) at 00:25:38 UT, showing a pre-event coronal environment. The paired images are scaled to the same image size, shifted to a common center, and rolled to the plane defined by the Sun center and the two spacecraft positions.

Table 1
Coordinate Information of the *STEREO* Twin Spacecraft at the Time of the Event

Parameter	*S/C B*	*S/C A*
Heliocentric distance (AU)	1.012520	0.967343
HEEQ[a] longitude (deg)	−22.599	21.092
HEEQ latitude (deg)	0.253	−5.177
Separation angle with Earth (deg)	22.800	21.168
Separation angle A with B (deg)	43.969	

Note. [a] HEEQ: Heliocentric Earth Equatorial coordinate system.

In the wake of the CME/flare event, large-scale disturbances are observed in the FOV of EUVI. Figure 2 shows the evolution of the EUV disturbances in 195 Å; in general coronal disturbing structures are better observed in 195 Å than in other wavelengths (Wills-Davey & Thompson 1999). We use running difference images (with a previous image in the sequence subtracted from every image) to enhance propagating changes. The first image showing discernable changes is taken at 00:45 UT; slight brightenings due to flare heating first occur in the flare site. At 00:55 UT the off-limb loop system above the flare site has evolved into a big bright loop that encloses a dark cavity. At its northern and southern sides diffuse brightenings appear on the disk (indicated by the arrows). In the following images, the bright loop expands and erupts out, and the diffuse brightenings propagate away from the flare site, leaving dimmings behind. As usually seen in an EUV wave, the propagation of the diffuse brightenings toward the bulk of the disk is largely obstructed by the equatorial CH; they propagate mainly northward and southward along the limb. The northern parts of the brightenings seem to move progressively to the backside of the disk so that later on only faint signatures very close to the limb can be seen. The southern ones are nevertheless more pronounced, with both off-limb and on-disk features observed over a large portion of the southeastern hemisphere. Because of the diffuse morphology it is not easy to accurately trace the propagation of the brightenings in the limb region. Rough estimation of their motion suggests a propagation speed of 260 km s^{-1}, which is among the typical velocities of EIT waves. At 01:25 UT, the propagating diffuse brightenings have stopped near the south pole, appearing as a stationary front. Plain images during this period (i.e., Figure 1) show that the stationary front is located at the boundary of the south polar CH.

One advantage of EUVI over previous EUV telescopes is that EUVI enables quasi-simultaneous observations in multiple wavelengths. Figure 3 shows almost simultaneous (within

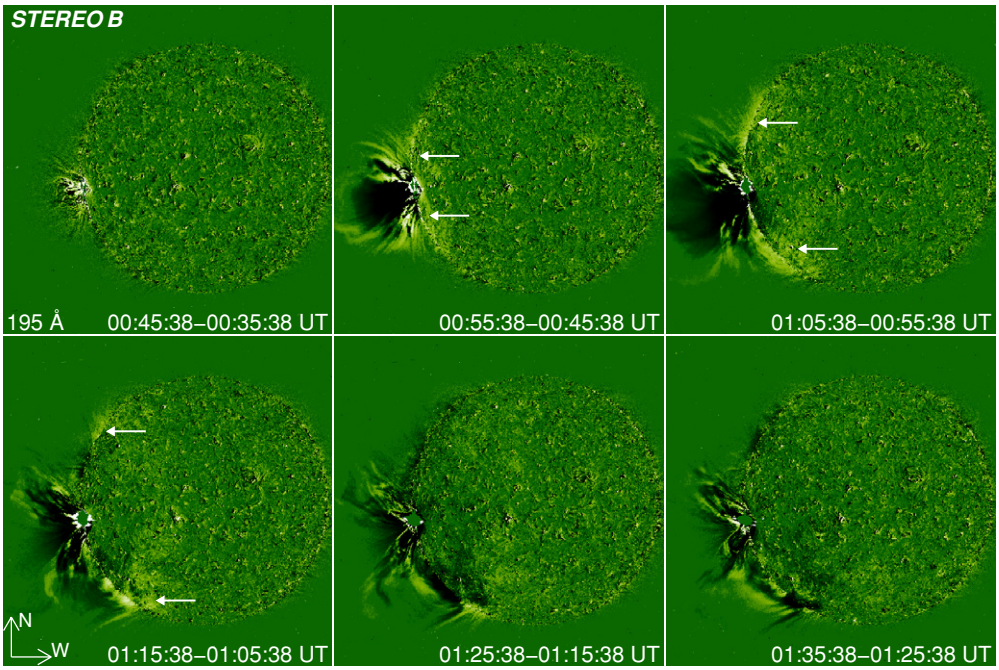

Figure 2. Running difference images of EUVI at 195 Å for *S/C B*. The arrows indicate the diffuse brightenings that propagate oppositely away from the flare site. Solar north is up, west to the right.

1 minute) running difference images of the large-scale disturbances in 171, 195, and 284 Å, the three coronal bandpasses of EUVI which cover the corona at temperatures around 0.9, 1.5, and 2.0 MK, respectively. To define the same changing features in different channels, the lowest cadence among the three bandpasses, 20 minutes, is set as the common time step. As can be seen from the figure, the disturbances are better identified in 195 Å; their propagation on the disk becomes barely observable when going to higher and lower temperatures. However, off-limb signatures of the disturbances are clearly observed in all bandpasses thanks to a lower background with less contribution from the disk. At around 01:06 UT (the middle panels in Figure 3), the off-limb disturbances occur at both sides of the erupting loop, appearing as dimmings, strong, and weak brightenings in 171, 195, and 284 Å, respectively. Since at around 00:46 UT no discernable brightening or dimming relative to the pre-event level at around 00:26 UT is seen outside the flare site in any EUVI bandpass, the dimmings (brightenings) at around 01:06 UT represent true emission depletion (enhancement) of the disturbances in the corresponding bandpasses. Changes in EUV intensity typically reflect changes in temperature and/or density of the emission medium. In this case, the multi-temperature behavior of the off-limb disturbances is mainly due to a heating process during which a large fraction of the coronal plasma in the disturbance region is heated to ~1.5 MK, a temperature close to the peak of the response function of the 195 Å line and within the descending (ascending) range of that of the 171 (284) Å line. The influence of possible mass enhancement on the EUV emission must be relatively marginal otherwise the disturbances would also be seen as brightenings in the 171 Å bandpass. At around 01:26 UT (the lower panels in Figure 3), a bright front is observed (also shown as the stationary front in the fifth frame in Figure 2) in all bandpasses (although in 171 Å the front is much weaker). Meanwhile the brightening (in 195 and 284 Å)/dimming (in 171 Å) pattern moves to the inner edge of the stationary front, indicating a movement of the heating source following the propagation the EUV disturbances. Behind the newly heated region, the same dimming behavior is evident in all bandpasses. Assuming a radiative cooling coefficient of $\sim 10^{-22}$ erg cm^3 s^{-1} at 1.5 MK (Raymond et al. 1976) and an electron density of $\sim 2 \times 10^8$ cm^{-3} for QS (e.g., Feldman et al. 1999), the cooling time for a temperature change of 0.5 MK is around 60 minutes, which is much longer than the time step adopted in Figure 3. This means that the temperature of the dimming region behind the stationary front does not decrease significantly from 01:06 UT to 01:26 UT. Hence, the dimmings seen in multiple wavelengths are more likely caused by mass draining from the lower corona. This outward mass transportation also results in some brightening features over the dimming region.

To link the EUV disturbances to the CME, four successive composite images of EUVI at 195 Å and COR1 in the interval of 00:55–01:25 UT (corresponding to the second–fifth frames in Figure 2) are shown in Figure 4. During the event the observation times of EUVI at 195 Å were the closest to those of COR1 (within 30 s) if we degrade the COR1 cadence by a factor of 2, making the combination of the two observations as physically reasonable as possible. Note that the quality of the EUVI images is degraded for the combined display. Since the FOVs of EUVI and COR1 overlap at 1.5–1.7 $R_\odot$, we manually choose a heliocentric height of 1.6 $R_\odot$ as the interface between the two FOVs. At 00:55 UT, the CME first appears as a small rim in COR1, which perfectly corresponds to the outermost part of the bright loop in EUVI. At 01:05 UT, a smooth transition of the CME is observed in the FOVs from EUVI to COR1. Cold prominence material with temperatures far from the effective response range of hotter coronal lines is seen in COR1 as a bright core, making the CME exhibit a typical three-part structure. Along with the radial propagation, a large lateral expansion of the CME is evident, especially during the period of 01:05–01:15 UT. Of particular interest is the appearance of a double-loop structure of the CME leading edge during the lateral

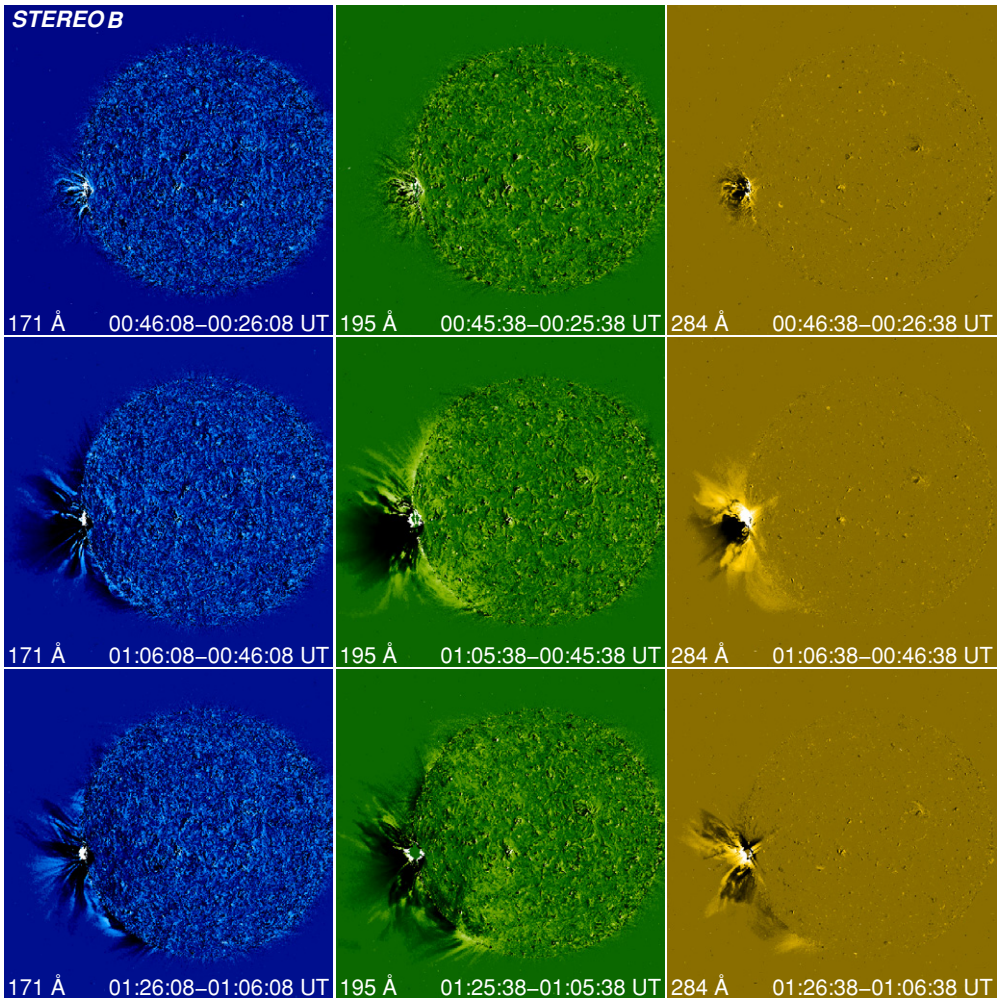

Figure 3. Twenty-minute running difference images of EUVI for *S/C B* at 171, 195, and 284 Å, respectively. Images in different bandpasses are taken almost simultaneously.

expansion. As pointed out by the arrows, the southern segment of the CME leading edge looks like consisting of two loops; each one extends smoothly down to the limb, with footpoints located at the flare site and the boundary of the south polar CH, respectively. Clearly, the EUVI–COR1 composite display shows a good consistency between the propagation of the EUV brightenings and the lateral expansion of the CME, although the CME legs appear thinner than the diffuse brightenings. The double-loop structure for the northern segment is rather elusive possibly due to interaction of the CME with a diffuse coronal streamer north of it. In addition, the footpoint of the northern segment may follow the northward propagating brightenings in EUVI to the backside of the disk. Therefore, the spatial correlation between the EUV disturbances and the CME in the northern hemisphere is not as definite as what we have obtained in the southern hemisphere.

Figure 5 shows X-ray and radio observations of the event. The *GOES* soft X-ray (SXR) light curve reveals a C8.3 class flare between 00:37 UT and 01:38 UT. The actual magnitude should be larger allowing for the partial occultation at near-Earth viewpoint. The SXR ascending phase can be separated into three parts: an impulsive increase to the first peak between 00:37 UT and 00:51 UT, a plateau between 00:51 UT and 01:02 UT, and a gradual increase to the main peak between 01:02 UT and 01:11 UT. The *RHESSI* mission misses the initial part of the hard X-ray (HXR) evolution due to the orbit night but records a peak at 00:48 UT. Then, the HXR intensity turns into an exponential decay except for some small bumps. Radio observations from Radio Solar Telescope Network (RSTN; 180–25 MHz) and *Wind*/WAVES (13.875–1.075 MHz) show rather complex emissions. The most pronounced feature is a strong type II burst starting from 00:53 UT, of which the harmonic band is much more prominent. Band splitting is evident in the harmonic emission; the upper band has a starting frequency of ∼110 MHz. The type II burst continuously drifts to lower frequencies, leaving imprints (most probably belonging to the fundamental band) in the decametric-hectometric (DH) domain around 01:18 UT. The relationship between the type II burst and the CME has been studied in detail by Liu et al. (2009). A group of type III emissions is seen from 01:00 UT, followed by another type II burst starting from 01:04 UT. Compared to the former one, the second type II burst is much weaker, with narrower frequency and time coverage. Accompanying the second type II burst are diffuse type IV bursts observable throughout the observing frequency range. Such a behavior is a rather typical one (for a comprehensive review, see Gopalswamy 2009).

To study spatial evolution of the energy release during the event, in Figure 6 we reconstruct two *RHESSI* images at energies of 15–30 keV in the intervals of 00:47:30–00:48:10 UT and 01:01:20–01:02:00 UT, which correspond to the main peak and

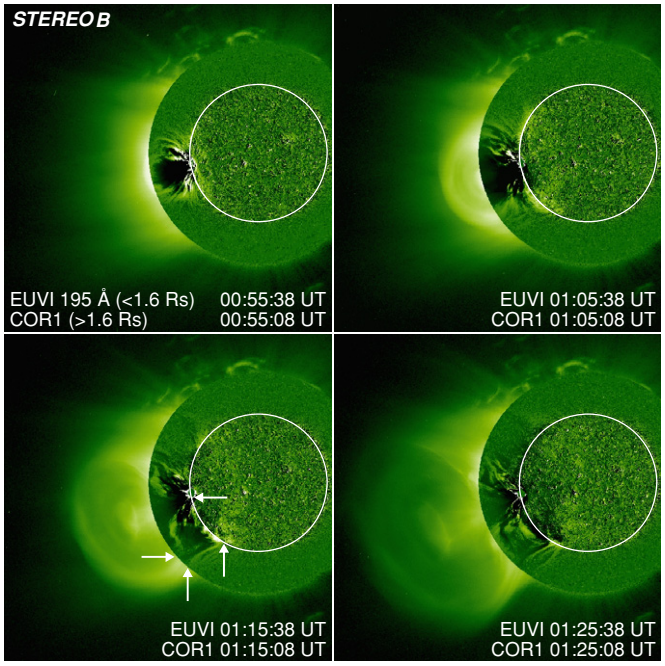

Figure 4. Composite images of EUVI at 195 Å and COR1 for *S/C B*. The corresponding running difference images in Figure 2 are adopted here for EUVI, but shown in a different intensity scale to enhance off-disk features, while plain intensity images are displayed for COR1. The arrows point out the double-loop structured CME leading edge and its footpoints on the limb, which are located at the flare site and the boundary of the south polar CH, respectively. The white circle represents the position and size of the solar disk.

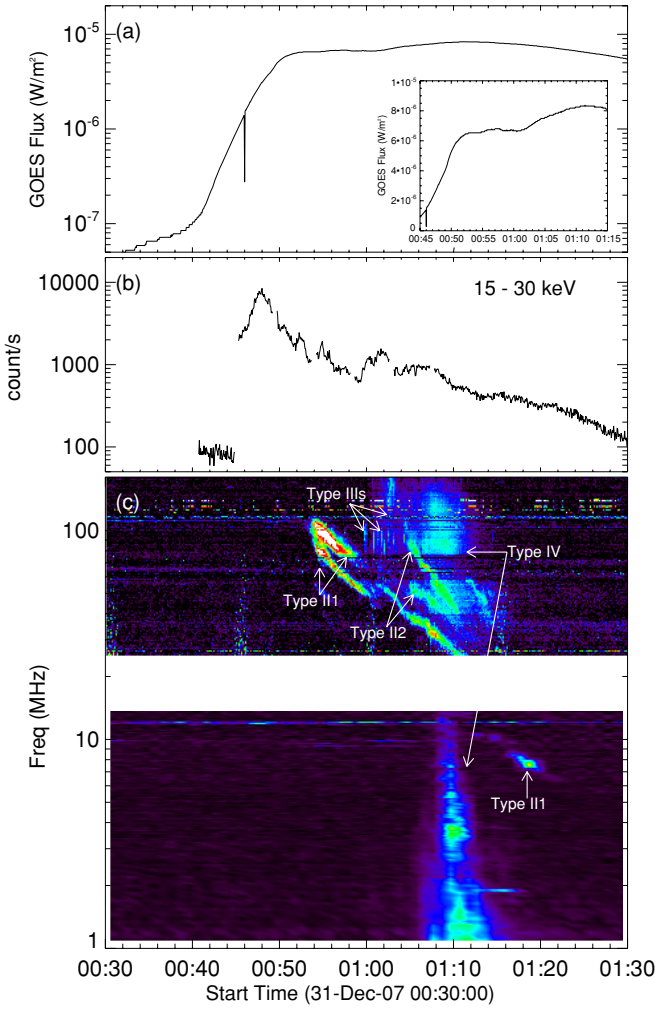

Figure 5. X-ray and radio observations of the event. The top two panels show *GOES* 1–8 Å SXR light curve and *RHESSI* HXR intensity profile at energies of 15–30 keV. The ascending part of the SXR light curve is re-plotted in linear scale in the inset for a better contrast. The bottom panel shows radio spectrum obtained by RSTN (180–25 MHz) and *Wind*/WAVES (13.875–1.075 MHz), respectively. The blank region in the middle means data gap between 25 and 13.875 MHz.

the most evident bump in the decay phase of the HXR light curve (as shown in Figure 5(b)), respectively. During the first period, a typical post-flare loop is seen, with two footpoints on the limb and a cusp structure on its top. The topology is consistent with the standard CSHKP model (Carmichael 1964; Sturrock 1966; Hirayama 1974; Kopp & Pneuman 1976). Although we cannot directly superpose the *RHESSI* images on EUVI images since the two observations are taken at different viewpoints, the near-limb location of the flare site can greatly minimize the projection effect. A rough co-alignment reveals that the HXR footpoints are cospatial with those of the EUV loop at 00:55 UT. In the second interval, the southern HXR footpoint moves southward along the limb by a distance of $\sim 20''$, while the northern footpoint has faded out. A new coronal HXR source appears southeast to the southern footpoint, indicating new reconnections between the CME/flare field lines and surrounding QS magnetic loops south of them. Due to the limited dynamic range of *RHESSI*, it is difficult to effectively reconstruct the possible reconnection-produced HXR source at the footpoints of the QS loops. Therefore, the apparent HXR source is rather compact compared with the more diffuse EUV brightenings. As the HXR intensity continuously decreases, no useful spatial information of the HXR source can be obtained.

3. DISCUSSION

EIT waves are usually an on-disk observed phenomenon. In the 2007 December 31 limb event, the large-scale EUV disturbances also show several typical characteristics of EIT waves: the diffuse brightenings (195 Å) propagate with a velocity of $\sim$260 km s^{-1}, and finally stop at the boundary of the south polar CH, leaving dimmings behind. The wave model considers EIT waves as a kind of density perturbation of the transmission medium without significant plasma heating. However, the different brightening/dimming behaviors of the propagating EUV disturbances in different wavelengths favor a heating process rather than a density enhancement in the disturbance region. By studying two on-disk events, Attrill et al. (2007) have recently proposed that EIT waves could be magnetic footprints of a CME on the disk. The EUVI–COR1 composite images of this limb event (Figure 4) show an unambiguous spatial correlation between the propagation of the diffuse brightenings and the large lateral expansion of the CME, providing more convincing evidence for their model. In such a scenario, reconnections between CME expanding magnetic field lines and surrounding favorably orientated QS magnetic loops cause a lateral expansion of the CME and brightenings at the laterally expanding CME footpoints; dimmings appear behind the brightenings as a consequence of volume expansion. Along with the lateral expansion, the CME leading edge evolves into a double-loop structure. Since the heated plasma does not cool down quickly during the CME lateral expansion, the brightenings will be rather diffuse compared with the relatively sharp CME legs. The event occurred at the solar minimum; a QS environment guarantees the existence of such QS magnetic

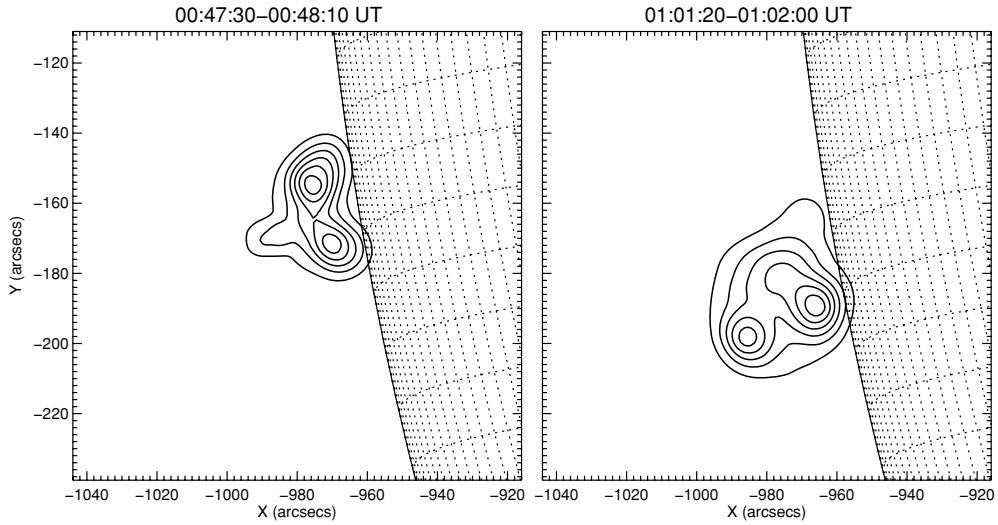

Figure 6. Reconstructed *RHESSI* images (with the Pixon algorithm) at energies of 15–30 keV in two intervals: during the main peak (left) and the most evident bump in the decay phase (right) of the HXR light curve in Figure 5(b). The nonthermal emission is shown in contours (15%, 30%, 45%, 60%, 75%, and 90% of the corresponding peak intensity for each panel).

loops outside the source region. Propagating brightenings will stop when they encounter open field lines (e.g., at the boundary of a CH). Either the open field lines are unfavorably orientated or the reconnections stretch the reconnected field lines to an infinite distance. In either case, a stationary front forms there. This may be the reason why CMEs generally keep a fixed angular span in their late phases. By use of EIT data, Chen (2009) has also found the above-mentioned cospatiality of "EIT waves" and CME leading loops in another limb event. Although he similarly proposed that "EIT waves" are produced by successive stretching of closed CME field lines rather than being real waves, without multi-temperature diagnostics (EIT mainly observes the Sun in the 195 Å channel) he concluded that the wave fronts are apparently moving density enhancements resulting from the magnetic perturbation.

Tracing the diffuse brightenings along the limb suggests that they should start to propagate between 00:55 UT and 01:05 UT. The timing is in agreement with the gradual increase in SXR from 01:02 UT, the most evident bump in HXR from 00:59 UT, and the complex radio emissions from 01:00 UT. Main magnetic reconnections in the flare site have turned into a decay since the initiation of the CME at ∼00:48 UT (derived from high cadence EUVI 171 Å observations of the event), but the CME expansion facilitates new reconnections between the CME field lines and surrounding QS magnetic loops. Such reconnections take place outside the main flare site, showing a displacement of the HXR emission sites (indicated in Figure 6). During the reconnections, the initially closed QS loops are "opened" to a high altitude; accelerated electrons escape along the reconnected field lines, producing Type III emissions. The two type II bursts in this event are believed to be generated by two shocks respectively: one driven at the CME front with a velocity over 600 km s^{-1} (Liu et al. 2009), and the other one at the CME flank due to the CME–QS loop interaction (Cho et al. 2008). If the EUV wave-like disturbances are the skirts of a true wave driven by the CME, we would expect a propagation velocity of the disturbances as high as 600 km s^{-1}, significantly higher than that measured (∼260 km s^{-1}) in this event.

As also can be seen in Figure 4, the double-loop structure of the CME leading edge develops as the CME propagates outward, indicative of a rotation with respect to the sky plane. This is consistent with the finding that the southern EUV disturbances are more prominent. (The northern ones may rotate to the backside of the disk.) Rotation of EIT waves has also been reported as an argument for the CME-related interpretation (Attrill et al. 2007). However, direct evidence of such a rotation relies on on-disk EUVI observations (Veronig et al. 2008; Long et al. 2008; Gopalswamy et al. 2009).

4. CONCLUSION

On 2007 December 31, a CME induced large-scale EUV disturbances along the limb which exhibit some typical characteristics of EIT waves such as a typical propagation speed of EIT waves and the formation of a stationary front at the boundary of a CH. By analyzing composite observations with EUVI and COR1 on board the *STEREO* mission and complementary X-ray and radio data of the event, we suggest that the wave-like EUV disturbances are a result of magnetic reconfiguration related to the CME liftoff rather than true waves in the corona. In this case, the unfavorable location of the source region prevents us from taking advantage of the capability of *STEREO* in stereoscopically viewing the Sun. However, with their increasing separation the *STEREO* twin spacecraft have now enabled us to observe both limb and on-disk signatures of an "EUV wave" if the source region is appropriately located. Several such cases have been reported since 2009. A work on the synthesis of these stereoscopic observations will be presented in a future paper and no doubt shed new light on the nature of such wave-like disturbances.

We are very grateful to the anonymous referee for his/her constructive and helpful comments. This work is supported by the French CNRS post-doctoral project "Observations and Modelisation of Coronal Mass Ejection Using *STEREO*, *SOHO* and *Hinode* Data." D.Y. and T.Y.H. are supported by NSFC key project no. 10333040 and NPBRS no. GYHY200706013 of China. We thank the *STEREO*/SECCHI, *GOES*, *RHESSI*, *Wind*/WAVES, and RSTN consortia for their open data policy.

REFERENCES

Attrill, G. D. R., Harra, L. K., van Driel-Gesztelyi, L., & Démoulin, P. 2007, ApJ, 656, L101
Aurass, H., Vourlidas, A., Andrews, M. D., Thompson, B. J., Howard, R. H., & Mann, G. 1999, ApJ, 511, 451
Biesecker, D. A., Myers, D. C., Thompson, B. J., Hammer, D. M., & Vourlidas, A. 2002, ApJ, 569, 1009
Carmichael, H. 1964, in AAS-NASA Symposium on Solar Flares, ed. W. N. Hess (NASA SP-50; Washington, DC: NASA), 451
Chen, P. F. 2006, ApJ, 641, L153
Chen, P. F. 2009, ApJ, 698, L112
Chen, P. F., Shibata, K., & Fang, C. 2005, ApJ, 622, 1202
Chen, P. F., Wu, S. T., Shibata, K., & Fang, C. 2002, ApJ, 572, L99
Cho, K.-S., et al. 2008, A&A, 491, 873
Cliver, E. W., Laurenza, M., Storini, M., & Thompson, B. J. 2005, ApJ, 631, 604
Delaboudinière, J.-P., et al. 1995, Sol. Phys., 162, 291
Delannée, C. 2000, ApJ, 545, 512
Eto, S., et al. 2002, PASJ, 54, 481
Feldman, U., Doschek, G. A., Schühle, U., & Wilhelm, K. 1999, ApJ, 518, 500
Gopalswamy, N. 2009, in Climate and Weather of the Sun–Earth System (CAWSES): Selected Papers from the 2007 Kyoto Symp., ed. T. Tsuda et al. (Tokyo: Terra Sci. Pub.), 77
Gopalswamy, N., et al. 2009, ApJ, 691, L123
Hirayama, T. 1974, Sol. Phys., 34, 323
Howard, R. A., et al. 2008, Space Sci. Rev., 136, 67
Kaiser, M. L., Kucera, T. A., Davila, J. M., St. Cyr, O. C., Guhathakurta, M., & Christian, E. 2008, Space Sci. Rev., 136, 5
Khan, J. I., & Aurass, H. 2002, A&A, 383, 1018
Klassen, A., Aurass, H., Mann, G., & Thompson, B. J. 2000, A&AS, 141, 357
Ko, Y.-K., Raymond, J. C., Lin, J., Lawrence, G., Li, J., & Fludra, A. 2003, ApJ, 594, 1068
Kopp, R. A., & Pneuman, G. W. 1976, Sol. Phys., 50, 85
Liu, Y., Luhmann, J. G., Bale, S. D., & Lin, R. P. 2009, ApJ, 691, L151
Long, D. M., Gallagher, P. T., McAteer, R. T. J., & Bloomfield, D. S. 2008, ApJ, 680, L81
Maia, D., Vourlidas, A., Pick, M., Howard, R., Schwenn, R., & Magalhães, A. 1999, J. Geophys. Res., 104, 12507
Moreton, G. E. 1960, AJ, 65, 494
Moreton, G. E., & Ramsey, H. E. 1960, PASP, 72, 357
Ofman, L., & Thompson, B. J. 2002, ApJ, 574, 440
Raymond, J. C., Cox, D. P., & Smith, B. W. 1976, ApJ, 204, 290
Sturrock, P. A. 1966, Nature, 211, 695
Thompson, B. J., Cliver, E. W., Nitta, N., Delannée, C., & Delaboudinière, J.-P. 2000a, Geophys. Res. Lett., 27, 1865
Thompson, B. J., Plunkett, S. P., Gurman, J. B., Newmark, J. S., St. Cyr, O. C., & Michels, D. J. 1998, Geophys. Res. Lett., 25, 2465
Thompson, B. J., et al. 1999, ApJ, 517, L151
Thompson, B. J., et al. 2000b, Sol. Phys., 193, 161
Thompson, W. T., et al. 2003, Proc. SPIE, 4853, 1
Uchida, Y. 1968, Sol. Phys., 4, 30
Veronig, A. M., Temmer, M., & Vršnak, B. 2008, ApJ, 681, L113
Veronig, A. M., Temmer, M., Vršnak, B., & Thalmann, J. K. 2006, ApJ, 647, 1466
Wang, Y.-M. 2000, ApJ, 543, L89
Warmuth, A., Vršnak, B., Aurass, H., & Hanslmeier, A. 2001, ApJ, 560, L105
Warmuth, A., Vršnak, B., Magdalenić, J., Hanslmeier, A., & Otruba, W. 2004, A&A, 418, 1117
Wills-Davey, M. J., DeForest, C. E., & Stenflo, J. O. 2007, ApJ, 664, 556
Wills-Davey, M. J., & Thompson, B. J. 1999, Sol. Phys., 190, 467
Wuelser, J.-P., et al. 2004, Proc. SPIE, 5171, 111
Zhukov, A. N., & Auchère, F. 2004, A&A, 427, 705